Microfluidic Handling on a Thermally Responsive Surface

Matthew R Clements
{clememr,karl}@ee.washington.edu

Dept of EE, University of Washington
Seattle WA, 98195-2500

Microfluidic Handling on a
Thermally Responsive Surface

by

Matthew R Clements

A project report submitted in partial fulfillment of the
requirements for the degree of

Master of Science, Electrical Engineering

University of Washington

2003

Program Authorized to Offer Degree: Electrical
Engineering

University of Washington
Graduate School

This is to certify that I have examined this copy of a master's project report by

Matthew R Clements

and have found that it is complete and satisfactory in all respects,
and that any and all revisions required by the final
examining committee have been made.

Committee Members:

_____

Karl F. Böhringer

_____

Tai-Chang Chen

Date: _____

Master's Project Report

In presenting this project report in partial fulfillment of the requirements for a Master's degree at the University of Washington, I agree that the Library shall make its copies freely available for inspection. I further agree that extensive copying of this thesis is allowable only for scholarly purposes, consistent with "fair use" as prescribed in the U.S. Copyright Law. Any other reproduction for any purposes or by any means shall not be allowed without my written permission.

Signature_____

Date_____

University of Washington

Abstract

Microfluidic Handling on a
Thermally Responsive Surface

by Matthew R Clements

Chairperson of the Supervisory Committee

Professor Karl F. Böhringer
Department of Electrical Engineering

Thermocapillary pumping is one promising method for generating flow in a microfluidics device. ppNIPAM is a plasma-deposited surface coating developed at the University of Washington. Experiments were conducted to determine ppNIPAM's ability to enhance thermocapillary pumping. A diode-pumped frequency tripled Nd:YAG laser (355nm) was used for fabrication. Silicon was optimally machined at 10kHz, 50mm/s, z=1100µm. Sapphire was optimally machined at 10kHz, 10mm/s, z=1600µm. An experimental setup for heating in the sub-hotplate regime (RT - 50°C with +/- 1°C resolution) is described and characterized.

TABLE OF CONTENTS

LIST OF FIGURES

Number

LIST OF TABLES

INTRODUCTION

Microfluidics has emerged in recent years as a solution for many areas of research. In the area of computation and infosecurity, microfluidic logic gates provide an alternative to charge-based computation with the benefit of eliminating a microprocessor's electromagnetic signature as a method of eavesdropping. In the area of biology, microfluidics is already used for large-scale combinatorial experiments at the dna-, protein- and cellular-level. With the founding of the Microscale Life Sciences Center (MLSC) at University of Washington in August 2001, microfluidics has become even more relevant to research taking place on campus.

Moving fluid through such devices, regardless of the application, requires a means of generating flow. Many methods have been presented in recent years including micromechanical[1] and electrohydrodynamic[2] pumping, electro-osmotic flow[3], electrowetting[4] and thermocapillary pumping[5]. However, many of these methods require interfaces to off-chip actuators or high-voltage power sources. To realize the maximum benefit of microfluidic devices, it will be necessary to generate flow using an on-chip device that can be incorporated into inexpensive fabrication processes.

Thermocapillary pumping (TCP) offers promise since it requires neither exterior mechanical actuation nor high voltage. TCP makes use of the Marangoni effect to direct droplet movement by applying a thermal gradient across the liquid-surface interface and creating shear stress at the liquid-air interface.

This study investigates the possibility of enhancing flow generation by combining conventional TCP with a dynamic surface chemistry.

A dynamic surface chemistry is provided by the plasma-polymerized *N*-Isopropylacrylamide (ppNIPAM) bio-coating developed at University of Washington Engineered Biomaterials (UWEB)[7]. ppNIPAM undergoes a phase transition at 29°C. As temperature increases past the transition point, ppNIPAM becomes more hydrophobic. Thus, ppNIPAM has the potential to enhance fluid movement induced by the Marangoni effect.

CHAPTER I: DEVICE THEORY

Surface tension is measured in units [dynes/cm] or, equivalently,

[mN/cm]. For a liquid droplet on a solid surface, there are three surface

forces at the liquid/solid/air interface. The three forces are related

according to Young's law, where θ_c is the contact angle:

$$\gamma_{sa} = \gamma_{sl} + \gamma_{la}\cos\theta_c \quad (\text{Eq. 1})$$
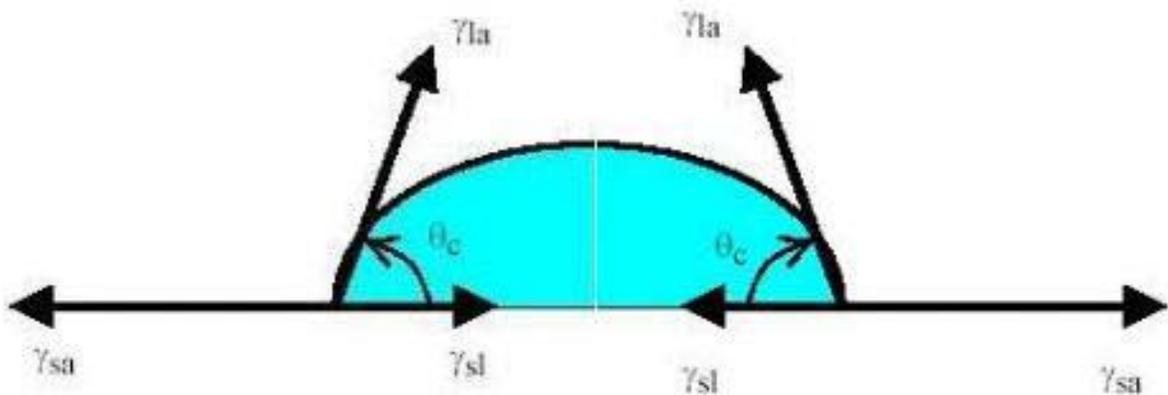

Figure 1: Liquid/Solid/Air interface; θ_c is the contact angle[6].

For hydrophilic surfaces $\theta_c < 90°$ and for hydrophobic surfaces $\theta_c > 90°$.

Although surface tension is often described by this diagram, the direction

of the force vectors sometimes causes confusion. For instance, if this

diagram is adopted to a capillary, the result is the diagram shown in

Figure 2.
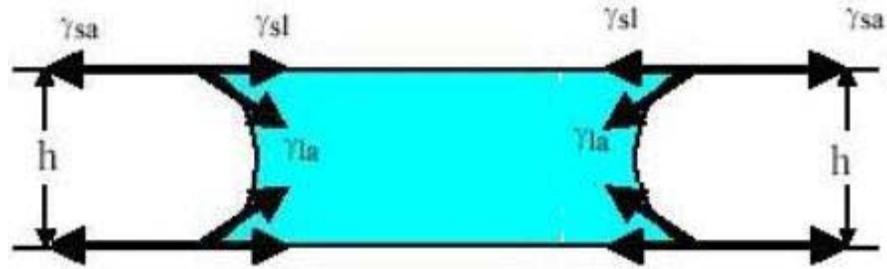
Figure 2: "Model One" of Capillary Forces

However, the direction of the force is not as Figure 2 illustrates. Figure 3 shows a hydrophilic capillary and the force due to surface tension where the force vector points away from the droplet, rather than towards it as in Figure 2.

$$F_{upward} = T 2\pi r$$

T = surface tension
ρ = density of liquid
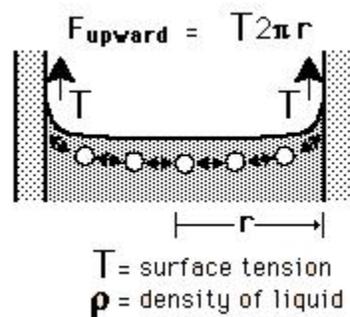
Figure 3: "Model Two" of Capillary Forces

This model is verified by the phenomenon of Thermocapillary pumping (TCP).   TCP operates by heating one end of a discrete liquid droplet. As the temperature rises at that end of the droplet, the surface tension

decreases at the solid-liquid interface. Surface tension decreases linearly with temperature according to the formula

$$\gamma = a - bT \quad \text{(Eq. 2)}$$

where a and b are positive empirical constants (for water, a=75.83 [dynes/cm] and b=0.1477 [dynes/cm/°C]). Therefore, force at the meniscus decreases linearly with temperature.

The decrease in surface tension reduces the lateral force on that side resulting in a net force on the droplet. In the case of hydrophilic channels, the droplet moves away from the heat (see Fig 4).
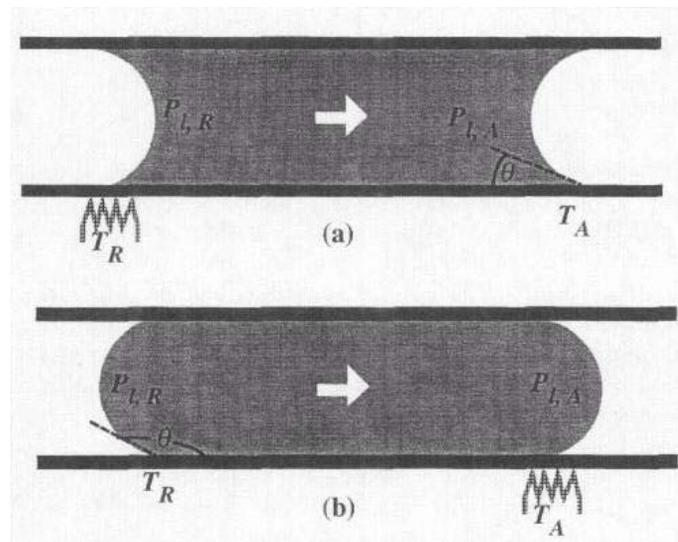
Figure 4: TCP of liquid drop in (a) hydrophilic channels and (b) hydrophobic channels[5].

Sammarco and Burns[5] have induced high drop velocities in mineral oil, toluene and water using temperature differences of 16–70°C (with room temperature as the baseline) in channels approximately 32µm x 500µm. Velocities increase linearly with temperature and require a minimum temperature difference of 5-20°C, depending on the liquid, before inducing any movement.

These empirical results indicate that Figure 2 is incorrect since Model One predicts a net force towards the hot end of the droplet, as shown in Figure 5, which does not occur in experimentation.
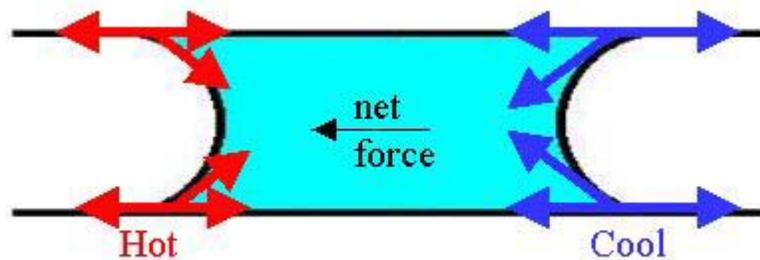
Figure 5: Model One predicts incorrect behavior of TCP

However, Model Two, with force vectors pointing away from the droplet as shown in Figure 6, accurately predicts the results empirically observed.
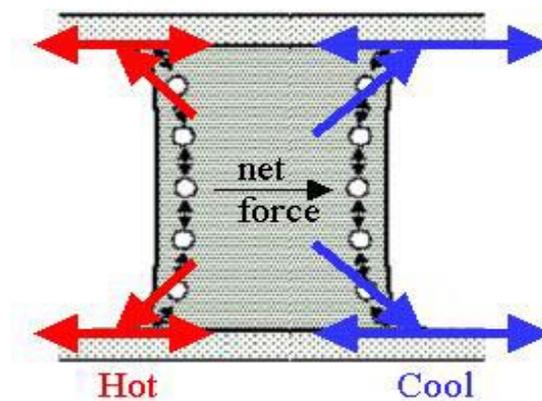
Figure 6: Model Two Predicts correct behavior of TCP

ppNIPAM

Plasma polymerized N-Isopropylacrylamide (ppNIPAM) is a surface

coating developed by the University of Washington Engineered

Biomaterials (UWEB) group. ppNIPAM undergoes a phase transition at

29°C as shown in Table 1[7].

Table 1: ppNIPAM phase transition

Temperature	Contact Angle
< 29°C	55°
> 29°C	75°

An increasing contact angle indicates a decreasing surface energy in the

hot state. The fluid atop the solid begins to bead since the surface

tension of the fluid is no longer so far below the surface energy of the

solid. If the surface tension of the fluid were to become greater than the surface energy of the solid then the contact angle would be >90°.

Since ppNIPAM is plasma deposited, it is possible to achieve a highly conformal coating on an irregular surface. In the case of surface-micromachined rectangular channels, all three sides will be coated conformally.

Hypothesis

In a ppNIPAM-coated channel, the hot end also becomes less hydrophilic resulting in an even larger net force on the droplet away from the heat as shown in Figure 7.
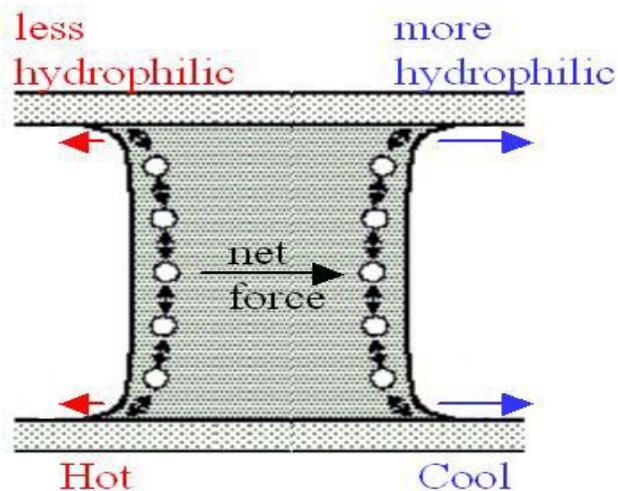


Figure 7: ppNIPAM cooperates with TCP effect

Thermocapillary pumping of discrete liquid droplets inside a ppNIPAM-coated microchannel should result in higher drop velocities than in microchannels of the same dimensions but with static surfaces.

CHAPTER II: FABRICATION

Microfluidic systems commonly employ transparent materials such as sodalime, mylar, and PDMS. Their transparency makes them easy to incorporate with optical-sensing techniques. PDMS, in particular, is commonly used because it allows for quick, inexpensive fabrication compared to traditional microfabrication techniques (lithography, etching, deposition, etc.).

To measure ppNIPAM's effect on the liquid-solid interface of a droplet, a simple, transparent channel is necessary to observe the dynamic behavior of the meniscus at each end of the droplet as ppNIPAM undergoes its phase transition.

However, the channel material must be compatible with the ppNIPAM deposition process. Using either PDMS or mylar contaminates the deposition chamber and compromises the integrity of the ppNIPAM. Thus, an alternative substrate is required.

Sodalime is inexpensive but is not common in microfabrication and therefore not well supported with recipes for wet-etching the required features. As an alternative to wet-etching, the department has a 355nm

near ultraviolet laser micromachining system. However, sodalime does
not absorb at 355nm, making good results difficult (See Fig 8).
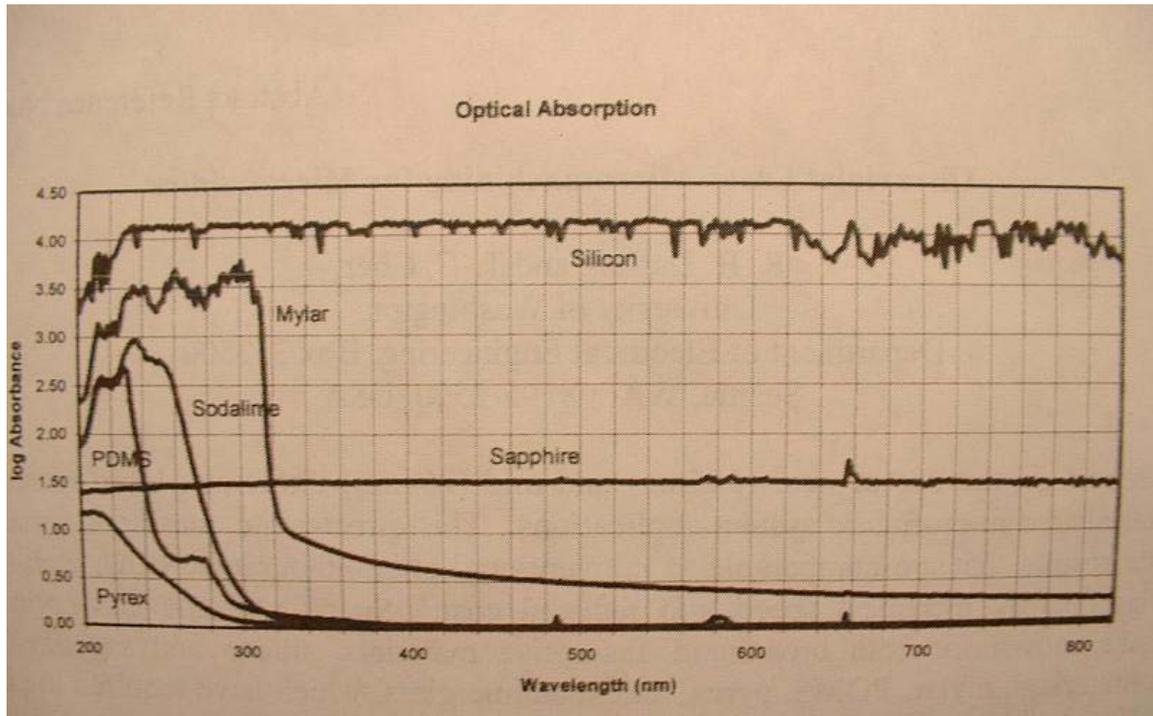
Fig 8: Absorption Spectra

Sapphire and Silicon both absorb at 355nm making them ideal
candidates for laser micromachining. Of course, there are well-
established wet-etching recipes for Silicon so it only makes sense to use
laser micromachining if it provides some advantage.

In principle, laser micromachining can significantly increase speed and
reduce cost over wet-etching, if comparable results can be achieved with
the proper parameters. We have gathered data on the effects of cutting

speed, laser pulse repetition rate, and focus plane on machined features in Silicon and Sapphire. This chapter will discuss those results and explain why the device was eventually implemented in Sapphire.

Laser Micromachining Theory

The mechanism of laser ablation is not well characterized. Generally speaking, ablation is the result of a photothermal process or a photochemical process or both.

The photochemical process is the result of high-energy photons breaking molecular bonds via photodissociation. The photothermal process is the result of lower-energy photons being absorbed by the lattice, creating phonons and, in turn, generating heat. This heat is dissipated through melting and vaporization. The ablation rate depends on photon energy and is slower for photochemical than for photothermal[8].

The relative contributions of the photothermal and photochemical processes are determined by the parameters: wavelength, power-density and pulse duration.

Wavelength should be matched to the material of interest. At 355nm, silicon and sapphire absorb well but materials like mylar, PDMS,

sodalime, and pyrex do not. In order to get good results with these materials it is necessary to use a 266nm laser.

As power density increases, vaporization dominates melt expulsion and the size of the evaporated particles decreases[9]. As power density continues to increase, the gas at the surface of the substrate becomes ionized and interferes with the coupling of laser energy, reducing resolution. This effect may be avoided with shorter pulse duration (ps or fs) such that there is not enough time for the plasma plume to form.

Additionally, with a fast pulse (ns, ps or fs) vaporization dominates but ablation rates are slow (<1μm/pulse). With slower pulses (ms) melt expulsion dominates yielding higher ablation rates (0.1 – several μm/pulse) but reduced resolution since the material reflows[9].

In addition to these laser-intrinsic parameters, several system-level operating parameters determine quality: focus, pulse repetition rate (rep-rate) and laser scan speed.

Moving the workpiece above or below the laser's focal-plane causes an increase in spot-size and thereby reduces the power-density. While one might assume that the best results occur at the focal-plane, Mai & Nguyen found that the optimum focal position using an Nd:YAG laser at

1064nm was 100μm below the surface[8]. Using the same wavelength, Dauer, et al., found the optimal focal position to be 500μm-1mm below the top wafer surface. Deviations from this position by +/-1.2mm resulted in a 20% reduction of the cutting depth. Using a 532nm wavelength resulted in an optimum focal position 300μm below the surface and a smaller tolerance of +/-100μm for 20% reduction of cutting depth[10]. Obviously there is substantial variation between authors. This is due partly to reliance on empirical interpretation but also indicates the immaturity of laser micromachining theory in general.

Pulse repetition rate (rep-rate) is the number of pulses delivered to the workpiece per time. As rep-rate increases, peak power decreases. Thus, ablation rate [μm/pulse] decreases as rep-rate increases.

Scan speed is the speed with which the workpiece is moved beneath the laser. As scan speed increases, there is less overlap between successive pulses. With less overlap between pulses, there is more variation in bottom and sidewall profiles.

No single combination of these parameters will provide the optimum process time, resolution, and surface quality. High resolution and surface quality come at the expense of slower ablation rates and thus longer processing times. However, since laser processing is a direct-

write, maskless process it is possible to fabricate all of the necessary structures without several cycles of masking and wet-etching, making all laser processing times relatively short in comparison.

Laser Setup

The department operates an ESI 4440 laser positioning system with an LWE 210 diode-pumped frequency-tripled Nd:YAG laser (355nm). The ESI 4440 allows 2500µm of movement in the z-axis to focus and de-focus the beam on the substrate. The x-y stage allows scan speeds from 0 – 250 mm/s. A vacuum nozzle in close proximity to the stage is used to remove debris.

The LWE 210 is a diode-pumped frequency-tripled Nd:YAG laser with a wavelength of 355nm. The laser was operated at 30 Amps. The laser spot size is 8.5µm (diameter) at focus. The laser pulse duration is ~20ns. Rep-rates range from 10,000 pulses/s to 30,000 pulses/s. Operating outside of this range reduces the lifetime of the laser.

Power density is calculated in the following way (using a 10kHz Rep-rate as an example):

Power/Pulse (PPP) = AvgPower/RepRate = 5W/10kHz = 5E-4 J

Peak Power (PP) = PPP/PulseDuration = 5E-4J/20E-9s = 25kW

Power Density(PD) = PP/SpotSize = 25kW/5.6E-7cm^2 = 44GW/cm^2

Fluence = PD x PulseDuration = 44GW/cm^2 x 20E-9s = 892J/cm^2

Average Power varies inversely with rep-rate. For the LWE 210, the power is approximately such that AvgPower=5W at 10k, 3.5W at 20k, and 1.5W at 10k.

Characterizing Silicon and Sapphire

Four trials were conducted to determine the effects of focus, scan speed, and pulse repetition rate on both silicon and sapphire.

In trial 1, a focus routine was run nine times using nine different combinations of scan speed and rep-rate. The focus routine moved the Silicon wafer (526µm thick) from 0µm to 2500µm in 100µm increments, cutting a 1mm line at each increment. A profilometer was then used to measure the depths of each cut. The optimum height was taken to be the height at which the depth was deepest for each combination of scan speed and rep-rate. For several combinations the profilometer showed only above-surface features and no cutting into the wafer. The results of those combinations are labeled "Inconclusive". See Appendix 1 for raw profilometer data and plots. The results are shown in Table 1:

Table 2: Trial 1, Stage height for single line cuts

Scan Speed [mm/s]	Rep Rate [Hz]	Optimum Height [µm]
10	10k	Inconclusive
50	10k	Z=300, 1400
100	10k	Z=400, 1400
10	20k	Inconclusive
50	20k	Z=200, 1500
100	20k	Z=200, 1800
10	40k	Inconclusive
50	40k	Inconclusive
100	40k	Inconclusive

The results from trial 1 indicate that, at 40kHz, the power density is too low to cut Silicon. The results also indicate that in all conclusive cases, there are two heights that are equally effective. The cause is unknown.

In trial 2, the same focus routine was run again on Silicon and additionally on Sapphire. Since 40kHz proved ineffective in trial 1, the combinations of trial 2 were limited to 10kHz and 20kHz with the same combinations of scan speeds. Although Sapphire had not been used in trial 1, it was not deemed necessary to test with 40kHz since it is even harder to cut than Silicon. Between trials 1 and 2, an alumina stage plate was added to the stage chuck in order to prevent laser-cutting of the chuck when drilling through substrates (as required by other procedures using the laser at that time). The alumina stage plate was 1000µm thick. The laser optics were re-focused before conducting trial

2. See Appendix 1 for raw profilometer data and plots. The results are shown in Table 2.

Table 3: Trial 2, Stage height for single line cuts

	Scan Speed [mm/s]	Rep Rate [Hz]	Optimum Height [µm]
Silicon	10	10k	Z=2500
	50	10k	Z=400, 1300
	100	10k	Z=300, 1300
	10	20k	Inconclusive
	50	20k	Z=200, 1700
	100	20k	Z=200, 1600
Sapphire	10	10k	Z=1000
	50	10k	Z=1200
	100	10k	Z=1300
	10	20k	Inconclusive
	50	20k	Inconclusive
	100	20k	Inconclusive

The results from trial 2 indicate the same trend in silicon whereby two focus heights, approximately 1-1.5mm apart are equally effective, reinforcing the results of trial 1. Again, some combinations produced only above-surface features, particularly 20kHz rep-rates in sapphire. These results were labeled "Inconclusive." It is proposed that power-density at 20kHz is too low to cut sapphire repeatably and predictably.

The purpose of trial 3 was to gather data on rastered boxes, rather than single lines, since rastering is the method of fabricating channels for the microfluidics device under investigation. All six combinations for both silicon and sapphire were repeated with rastered boxes. From the focus

data of trials 1 and 2, the ranges of z-height were narrowed for each material. Sapphire was studied at 800µm, 1100µm, and 1400µm. Silicon was studied at 600µm, 1100µm, and 1600µm. For each combination of scan speed and rep-rate, the depth of the rastered box at each z-height was plotted. The height at which the rastered box was both deep and uniform was taken to be the "Optimum Height".

A note on uniformity: uniformity statistics are not available for a 2-D scan of the bottom of the box. Only the 1-dimensional profilometer scan yields any indication of uniformity. Since boxes are rastered line by line, the wafer may become oriented in the profilometer such that the stylus traverses the parallel-running hillocks left by the laser and shows up as an oscillation in the 1-D scan. This fact limits the reliability of 1-D profilometer scans as an indication of uniformity. However, no 2-D uniformity statistics are available so the 1-D scans are appealed to in their absence. See Appendix 1 for the raw profilometer data and plots. The results are shown in Table 3:

Table 4: Trial 3, Stage height for Rastered Boxes

	Scan Speed [mm/s]	Rep Rate [Hz]	Optimum Height [µm]
	10	10k	Inconclusive +
	50	10k	**Z=1100**
Silicon	100	10k	Z=1100
	10	20k	Inconclusive +
	50	20k	Z=1600

	100	20k	Z=1100
	10	10k	**Z=1600**
	50	10k	Z=1600
Sapphire	100	10k	Z=1100
	10	20k	Z=1400
	50	20k	Z=1400
	100	20k	Z=1400

Sapphire yields better results at an even higher z-height than trial 2 indicated. In all combinations, the highest z-height produced the best results. Two combinations were cut at Z=1600 by mistake, but these proved the most uniform. Of all combinations, 10/10k produced the deepest and most uniform box.

Silicon yields better results at 1100µm than at 600µm or 1600µm. At low scan speeds, only above-surface features exist. It is speculated that this is the result of a boiling effect whereby the molten material boils up and then cools, recrystallizing as a bubble above the surface. Of all combinations, 50/10k produced the deepest and most uniform boxes.

The results of trial 3 indicate that laser machining produces more uniform results in sapphire than in silicon. Therefore, sapphire was chosen as the substrate for machining the microfluidics device under investigation.

Trial 4 was conducted to determine the effects of scan speed and rep-rate on depth. Two combinations, 20/10k and 50/10k, were run at varying

heights while all other combinations were run at Z=1600. The best results, those in Table 4 below, were all at Z=1600. The profilometer was used to map the depth of the boxes. See Appendix 1 for profilometer data and plots.

Table 5: Trial 4, Boxes in Sapphire

Scan Speed [mm/s]	Rep Rate [Hz]	Reps	Depth [μm]
5	10k	1	~76um (+/-3um)
10	10k	1	~38um (+/- 2um)
10 (2 reps)	10k	2	~76um (+/- 4um)
20	10k	1	~19um (+/- 2um)
50	10k	1	~8um (+/- 1um)

The results of trial 4 incorporate a new parameter, "Reps". This is the number of times the routine executed. When the laser rastered a box twice rather than just once, the result was a box twice as deep. This was expected. Uniformity was generally very good with each combination but particularly for 10/10k considering variation as a percentage of box-depth.

Microfluidic Device Machining

All combinations of scan speed and rep-rate used in trial 4 were subsequently used to machine the first devices. A 3" sapphire wafer was diced into 4 quarters. On the first of these quarters, four devices were machined using the four combinations shown in Table 4. The device dimensions were all identical and were as shown in Figure 5:
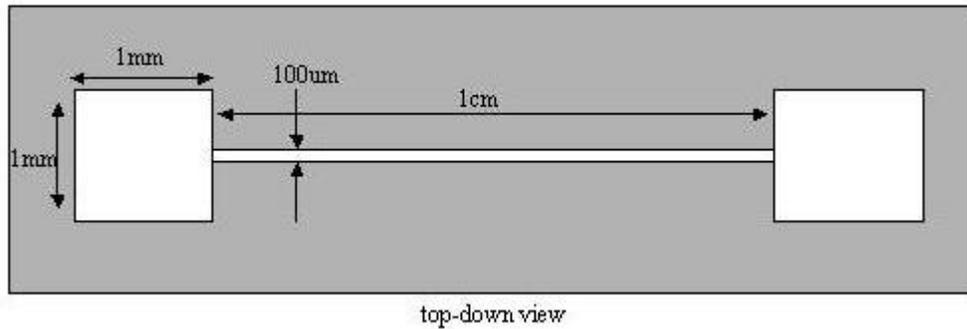
Figure 9: Device Dimensions

ppNIPAM deposition

Prior to deposition, all debris was removed using Acetone, IPA, DI water
and drying with nitrogen. The wafer was then delivered to the UWEB
lab, where Xuanhong Cheng processed the wafer in the ppNIPAM plasma
chamber.

PDMS

A PDMS mold was fabricated to serve two purposes: (1) seal the tops of
the channels, and (2) provide an inlet/outlet interface. Teflon tubing
molded into the PDMS provides the interface between fluid reservoir and
channel as shown in Figure 6:

Teflon tubing, ID 0.02" (508um)

~12 in

PDMS

20um, 40um, 80um

sapphire
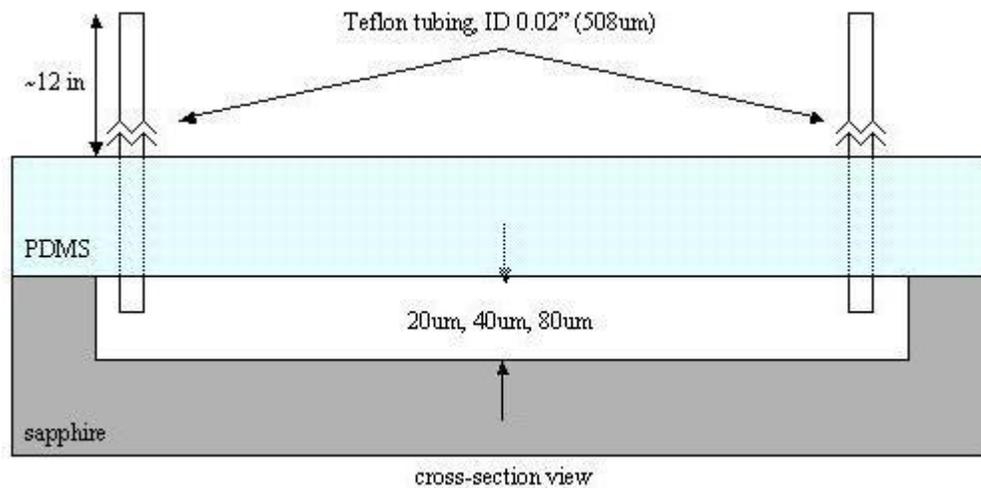
cross-section view

Figure 10: Cross-section of PDMS cap

PDMS is a two-part silicone elastomer. After mixing Parts A and B, and removing bubbles by vacuum, the mixture was poured onto a polyurethane block in which two steel pins (0.024" diameter) were embedded. Teflon tubing, with a 0.02" inner diameter, was fixed to each of the steel pins. This apparatus was cured at 25°C for 72hrs over the weekend. For faster results, PDMS may also be cured at 55°C for 3hrs.

Subsequent PDMS molding was done on a silicon wafer with embedded steel pins. The steel pins were UV-glued into 1mm holes drilled by the laser. The silicon wafer broke during application of the dam to contain the liquid PDMS. Silicon shards remained on PDMS after curing.

CHAPTER II: EXPERIMENT

Two experiments were conducted: 1) a glass-slide experiment, and 2) a

sapphire channel experiment. The purpose of the first experiment was to

verify that ppNIPAM's change in surface energy affected the meniscus in

a capillary. The purpose of the second experiment was to check for

unexpected effects in a continuous channel of fluid.

Heating in the sub-hotplate regime

The temperature range of interest (around 29°C) is too low for hotplates,

which typically operate at or above 60°C. An experimental apparatus

was devised to control heat in the range between room temperature and

~50°C. A GE 250W Infrared light bulb in a reflector fixture was used to

heat the device. The apparatus is shown in Figure 7.
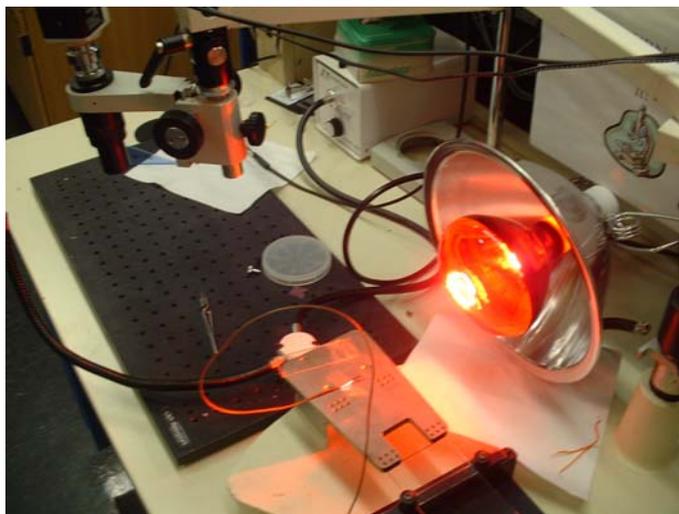
Figure 11: Heating Apparatus

The lamp illuminates from the side of the stage to allow for the CCD

camera (top left of Figure 6) to record the meniscus from above the stage.

The equilibrium temperature of the device on the stage depends on the

distance of the lamp to the stage. The air temperature was measured

5mm above the stage as the distance was increased from 40mm to

140mm. The distance was measured from the thermocouple to the

center of the bulb. The k-type thermocouple plugged into a Fluke 80TK

adapter. The adapter plugged into a Radioshack DMM interfaced to a PC

running Meterview 1.0.
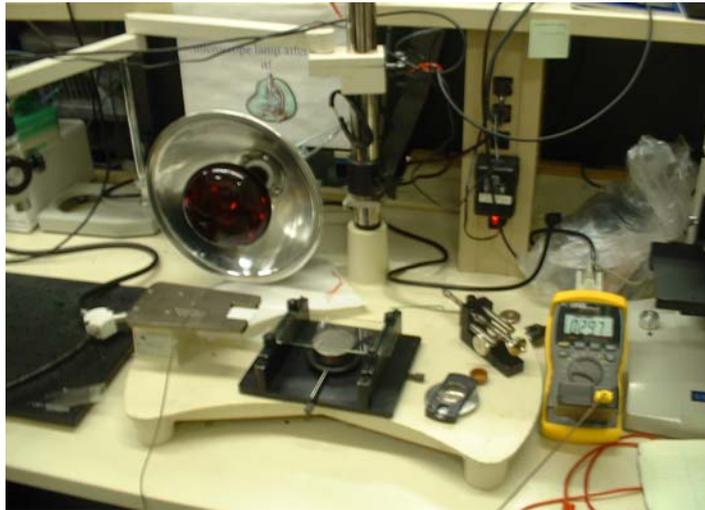
Figure 12: Data-logging setup
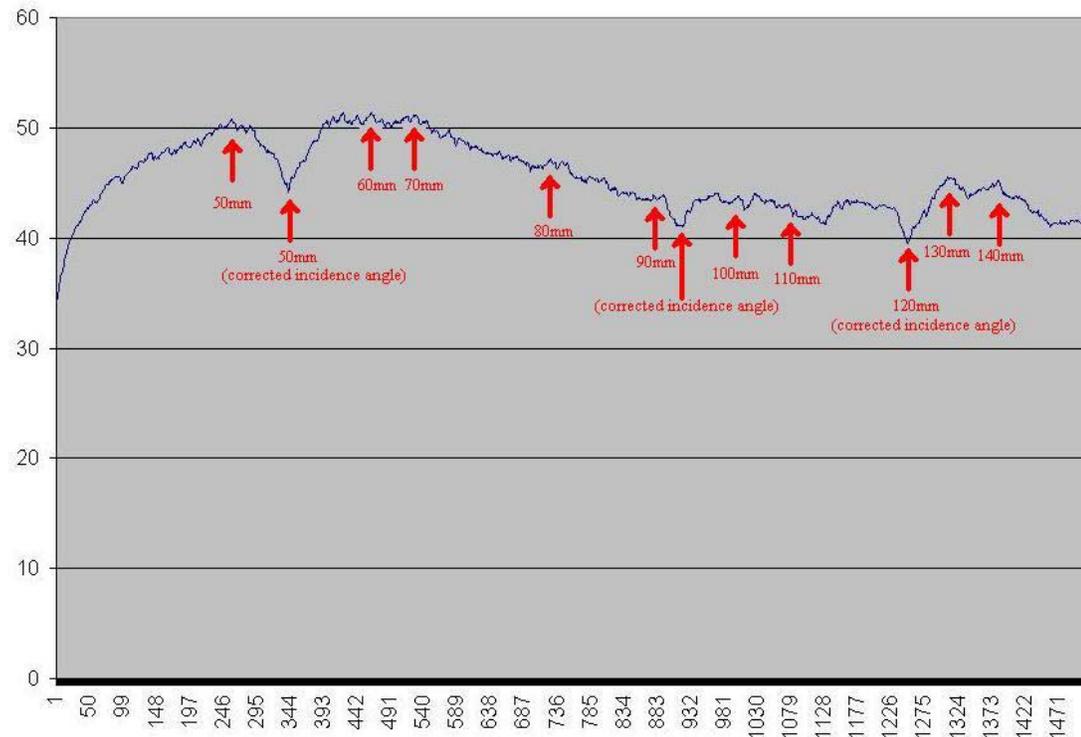
Figure 13: Equilibrium temps between 40 and 140mm distance

The noise in the data in Figure 9 is attributable to three things: (1) incidence angle, (2) air currents, and (3) proximity of thermocouple to stage.

Incidence angle is the largest source of error. For instance, after adjusting the lamp to 50mm temperature drops sharply. Upon inspection, the lamp had moved off-axis such that the center of the lamp no longer pointed toward the stage. After re-aiming the lamp, the temperature then returned to its earlier range (above 50°C).

Air currents are also a source of error. Temperatures never stabilized better than +/- 1°C. Fluctuations in temperature were noticed when people walked nearby and when air exchangers came on in the room.

The thermocouple also reports a lower temperature closer to the stage. All free air measurements were done at 5mm above the stage. Since the stage has much considerable thermal mass it stays cooler than the air above it.

Two different types of temperature response curves were measured: (1) free air, and (2) glass substrate. All measurements were conducted at 125mm in order to raise the temperature to approximately 40°C.
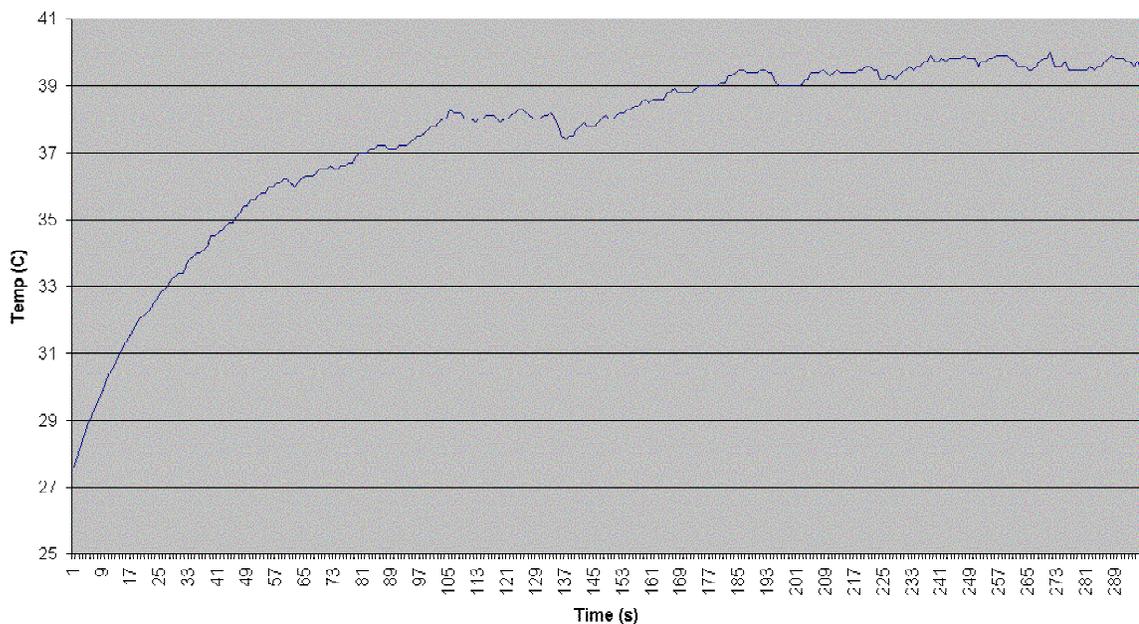

Figure 14: Heating in free air from 125mm distance
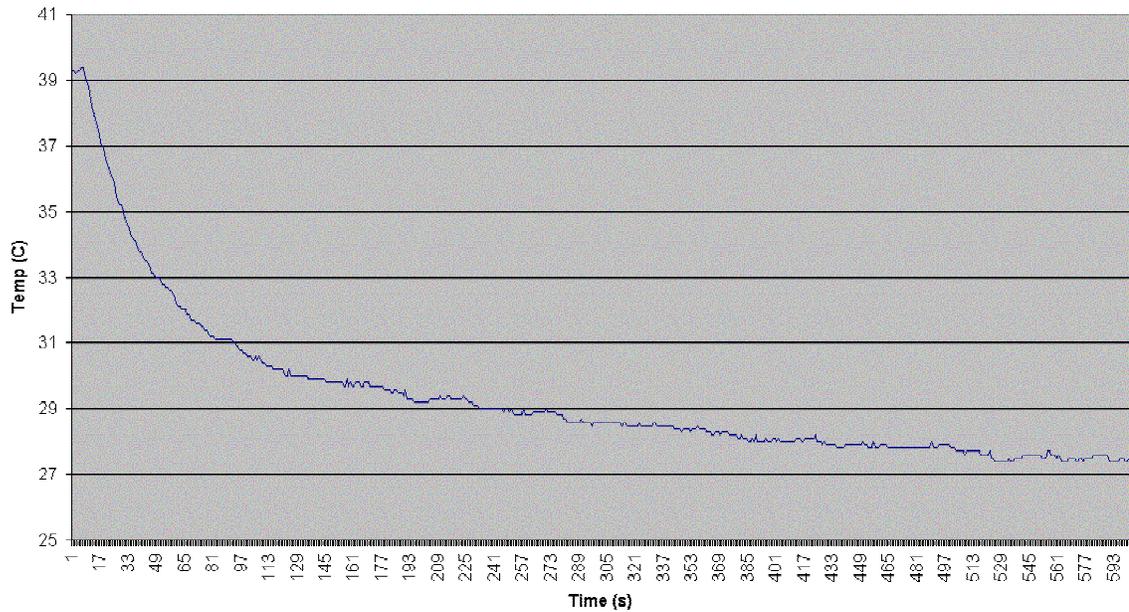
Figure 15: Cooling in free air

In Figures 10 and 11, equilibrium temp is 40°C. The temperature

difference is 13°C and the air reaches 63.2% (35.2°C) in 47s. Cooling

down reaches 36.8% of the difference (31.8°C) in 68s.
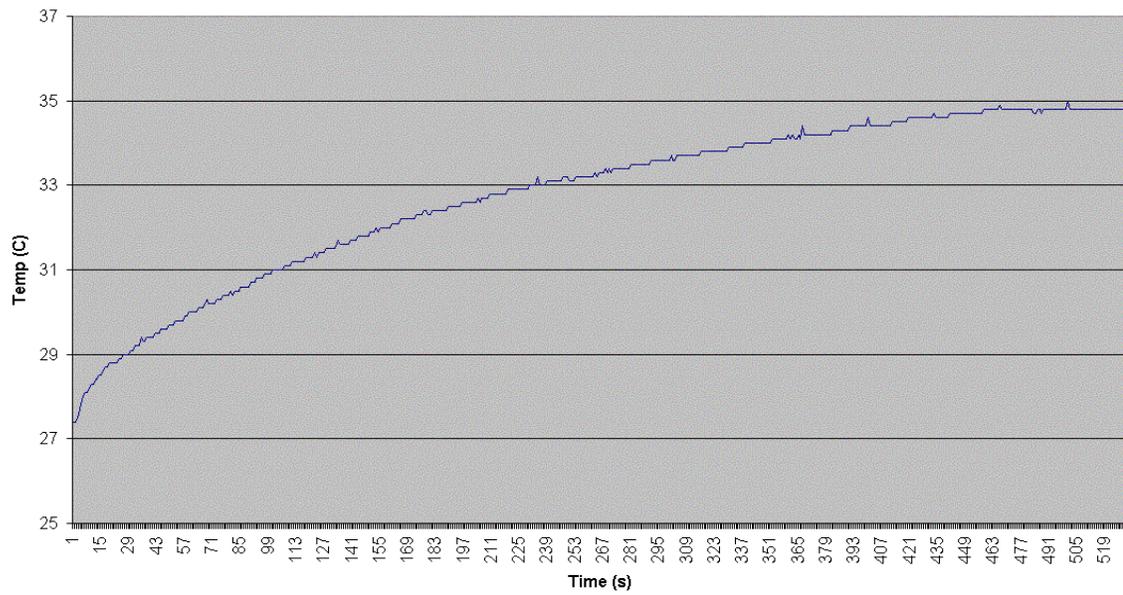
Figure 16: Heating glass from 125mm distance
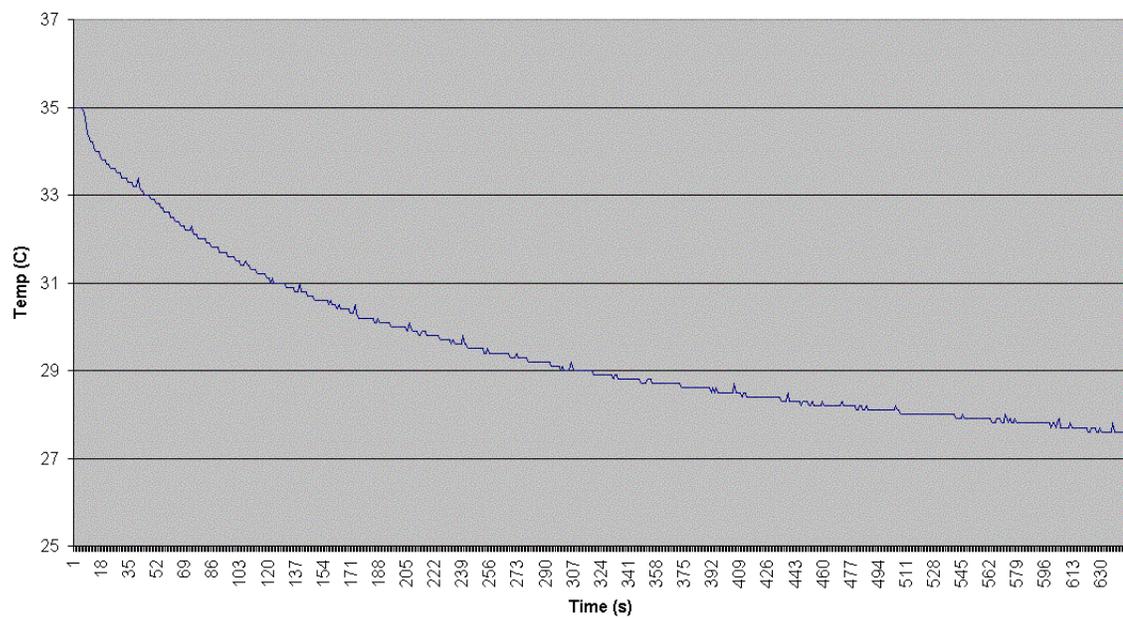
Figure 17: Cooling glass

In Figures 12 and 13, equilibrium temp is 35°C. The temperature difference is only 8°C and the glass reaches 63.2% (32.0°C) in 155s. Cooling down reaches 36.8% of the difference (29.9°C) in 215s.

In summary, the response time for the glass device is approximately three times longer than the free air response. The glass device also reaches a lower equilibrium temperature but one which is high enough to trigger the phase transition in ppNIPAM.

Glass Slide Experiment

By measuring the marching velocity of the capillary meniscus, it is possible to determine whether ppNIPAM enhances the interaction at the solid-liquid-air interface. Two devices, a test and a control, are injected with fluid at room temperature and the velocity is measured with a CCD camera and timer. Both devices are then heated to 35°C and injected with fluid at 35°C. If the meniscus in the ppNIPAM-coated capillary advances faster, it indicates that ppNIPAM's contribution is significant enough to enhance TCP.

Two glass slides were coated with ppNIPAM. Two pieces of double-sided tape were placed in parallel 500µm apart on the coated side of one slide. The second slide was then attached to form a channel approximately 75µm high by 500µm wide with ppNIPAM-coated surfaces on both top

and bottom. An identical device was constructed of non-coated glass slides to act as a control.

The device was placed flat on stage beneath a video camera. A syringe was used to inject green-dyed DI water into the test device and control device at room temperature. Both devices were then heated to 35°C. The meniscus of the test device receded slightly. However, the meniscus in both devices receded as the fluid rapidly evaporated under heat.   The volume of water in the channel was approximately 0.75µL.


Figure 18: Fluid evaporated in channel

The experiment failed to isolate ppNIPAM's contribution from evaporation's contribution.

Sapphire Channel Experiment

The principle of this experiment was to measure the effect of ppNIPAM, if any, on a continuously flowing channel of fluid. Pressure and flow-rate are measured in the test and control device at room temperature. Both

devices are then raised to 35°C and flow-rate is measured again for the same input pressure. The control device indicates the difference due to change in viscosity. Any additional difference in the test device is attributable to ppNIPAM.

Prior to pressure and flow-rate measurements, a syringe was used to inject green-dyed DI water into a channel.


Figure 19: PDMS-sapphire bond leaked

The fluid leaked between the PDMS and sapphire before generating enough pressure to exit the outlet. In the first trial, a small PDMS cap was even clamped to the sapphire with no success. In the second trial, a larger cap was made to increase adhesion but roughness from the broken silicon wafer prevented the PDMS from forming a tight seal.

CHAPTER III: CONCLUSION

A heating apparatus was devised to heat in the sub-hotplate regime. The apparatus ranges from room temperature to 50°C with +/1°C stability. Parameters were determined for machining uniform and consistent features in sapphire and silicon with the department's 355nm laser. The best results for silicon were achieved with a 10kHz rep-rate, 50mm/s scan speed, and stage height at 1100µm. This combination results in a cutting depth of 25µm +/-5µm. The best results for sapphire were achieved with a 10kHz rep-rate, 10mm/s scan speed, and stage height at 1600µm. This combination results in a cutting depth of 38µm +/-2µm. Experiments to determine the effect of ppNIPAM on TCP were inconclusive.

Future Work

Given more time, the glass slide experiment should be conducted in a humid environment to prevent evaporation or with a high boiling-point fluid, such as mineral oil.

The leaking PDMS might be overcome by casting on a very smooth polyurethane surface but most likely an alternative to PDMS is required. A box of sapphire should be coated with ppNIPAM and adhered to the top of the sapphire channels. This sapphire box would require thru-holes in

which Teflon tubing could be UV-glued. The rigid sapphire cap should withstand the pressure of the injected fluid.

As of this writing, the department now has a diode-pumped frequency quadrupled Nd:YAG laser (266nm) which is well suited for machining sodalime. Machining future channels in sodalime will allow quick and easy fabrication without the expense of sapphire.

BIBLIOGRAPHY

1. A. Hatch, A. E. Kamholz, G. Holman, P. Yager, K. F. Böhringer, A Ferrofluidic Magnetic Micropump. Journal of Microelectromechanical Systems, 10, June 2001.

2. Bart, S. F., Tarrow, L. S., Mehregany, M. & Lang, J. H. Microfabricated electrohydrodynamic pumps. Sensor Actuators A 21-23, 193-197 (1990).

3. Manz, A. et al. Electroosmotic pumping and electrophoretic separations for miniaturized chemical analysis systems. J. Micromech. Microeng. 4, 257-265 (1995).

4. C.-J. Kim, "Micropumping by Electrowetting", Int. Mechanical Engineering Congress and Exposition, New York, NY, Nov. 2001, IMECE2001/HTD-24200.

5. Sammarco, T. S. and M. A. Burns, "Thermocapillary Pumping of Discrete Drops in Microfabricated Analysis Devices," AIChE Journal, 45(2), 350 (1999).

6. L.J. Yang, T.J. Yao, Y.L. Huang, Y. Xu and Y.C. Tai," Marching Velocity of Capillary Meniscuses in Microchannels," Fifteenth IEEE International Conference on Micro Electro Mechanical Systems (MEMS '02), Las Vegas, USA, Jan. 20-24 (2002).

7. Pan, Y. V.; Wesley, R. A.; Luginbuhl, R.; Denton, D. D.; Ratner, B. D., "Plasma Polymerized N-Isopropylacrylamide: Synthesis and Characterization of a Smart Thermally Responsive Coating", Biomacromolecules; (Article); 2001; 2(1); 32-36.

8. T.A. Mai, N.T. Nguyen, Fabrication of micropumps with Q-switched Nd:YAG Lasers, 2nd Int. Symposium on Laser Precision Microfabrication LPM2001, Singapore, May 2001.

9. A. Luft, U. Franz, A. Emsermann, J. Kaspar: "A study of thermal and mechanical effects on materials induced by pulsed laser drilling", Appl Phys A 63 (1996) 2, 93-101.

2

10. S. Dauer, S. Büttgenbach, A. Ehlert; "Rapid Prototyping of Micromechanical Devices Using a Q-Switched Nd:YAG Laser with Optional Frequency Doubling", Conf. Proc. Eurosensors XII, Southampton, 13.-16.9.1998, Vol. 1, pp. 7-10.

**APPENDIX A: Absorbance Plots**

Sample Name : PtTFPP
Solvent Name : MeCl
Concentration :   1.0000
Units   :

Function   : Absorbance
Wavelength Range : 200 to 820 nanometers
Integration Time : 1 seconds
Std Deviation   : OFF
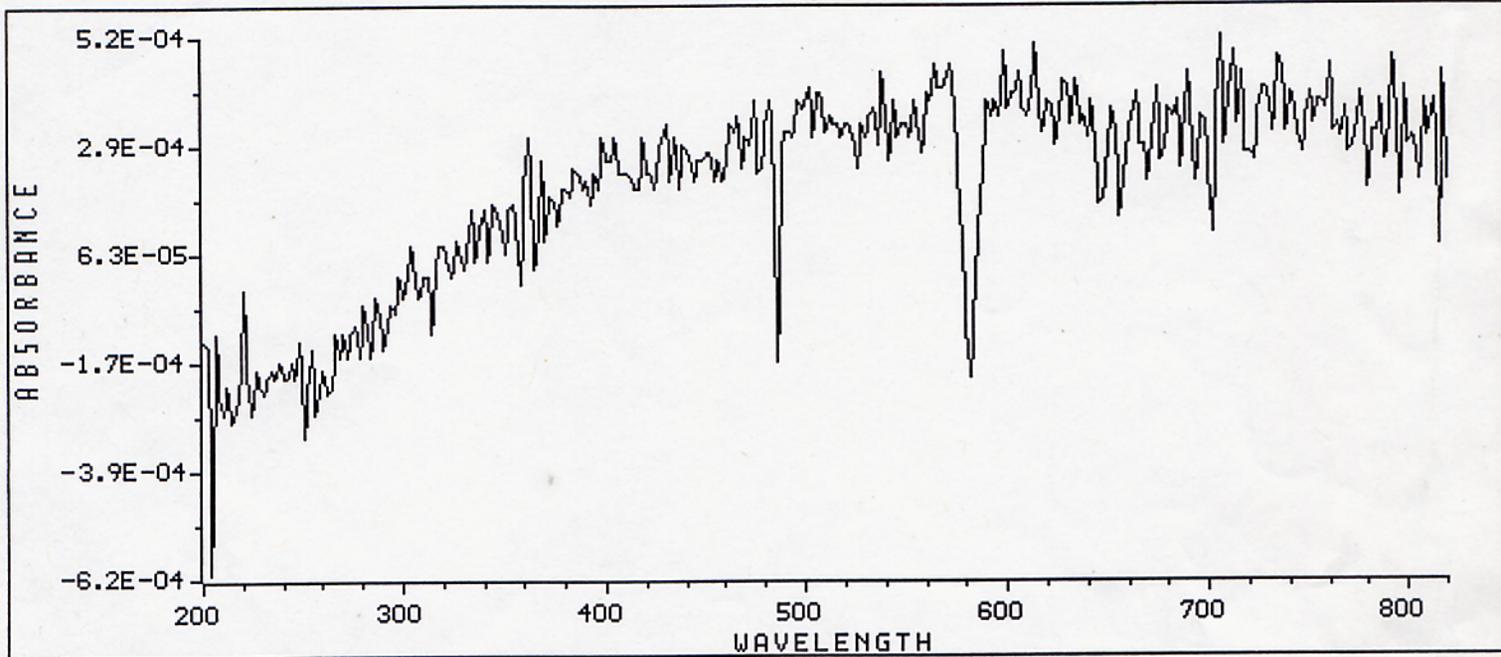
Background

Sample Name : PtTFPP   Function   : Absorbance
Solvent Name : MeCl   Wavelength Range   : 200 to 820 nanometers
Concentration :   1.0000   Integration Time   : 1 seconds
Units   :   Std Deviation   : OFF
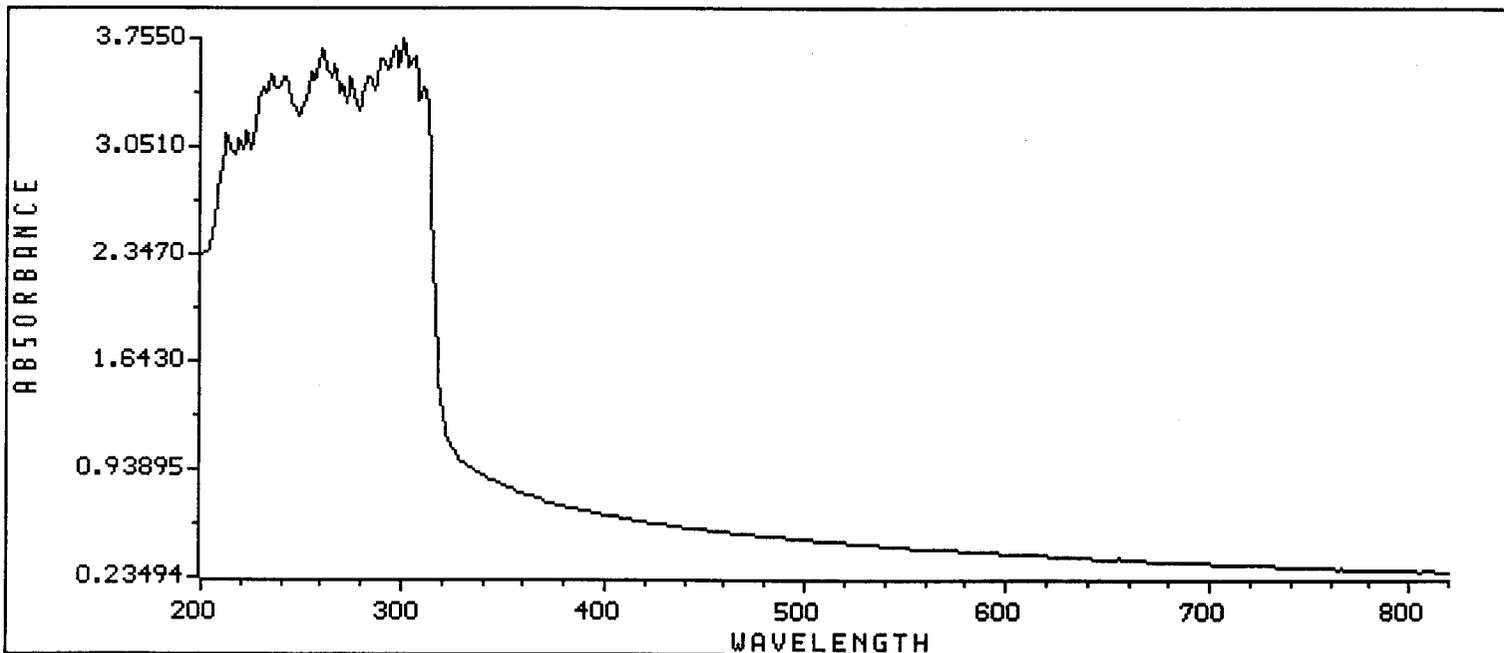
Mylar

Date   : 11-18-2002
Time   : 14:47:20
Operator : none

Sample Name   : PtTFPP
Solvent Name   : MeCl
Concentration :   1.0000
Units   :

Function   : Absorbance
Wavelength Range : 200 to 820 nanometers
Integration Time : 1 seconds
Std Deviation   : OFF
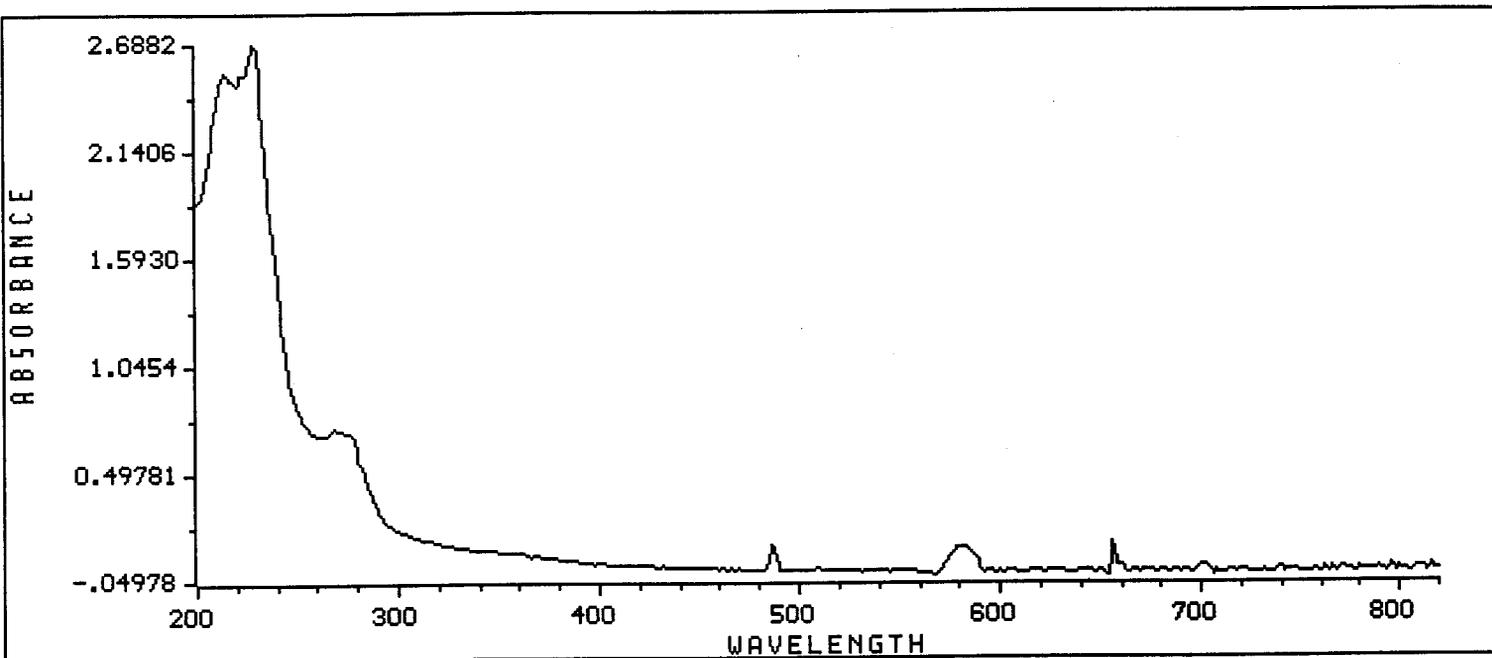
PDMS

Sample Name : PtTFPP
Solvent Name : MeCl
Concentration :   1.0000
Units   :

Function   : Absorbance
Wavelength Range : 200 to 820 nanometers
Integration Time : 1 seconds
Std Deviation   : OFF
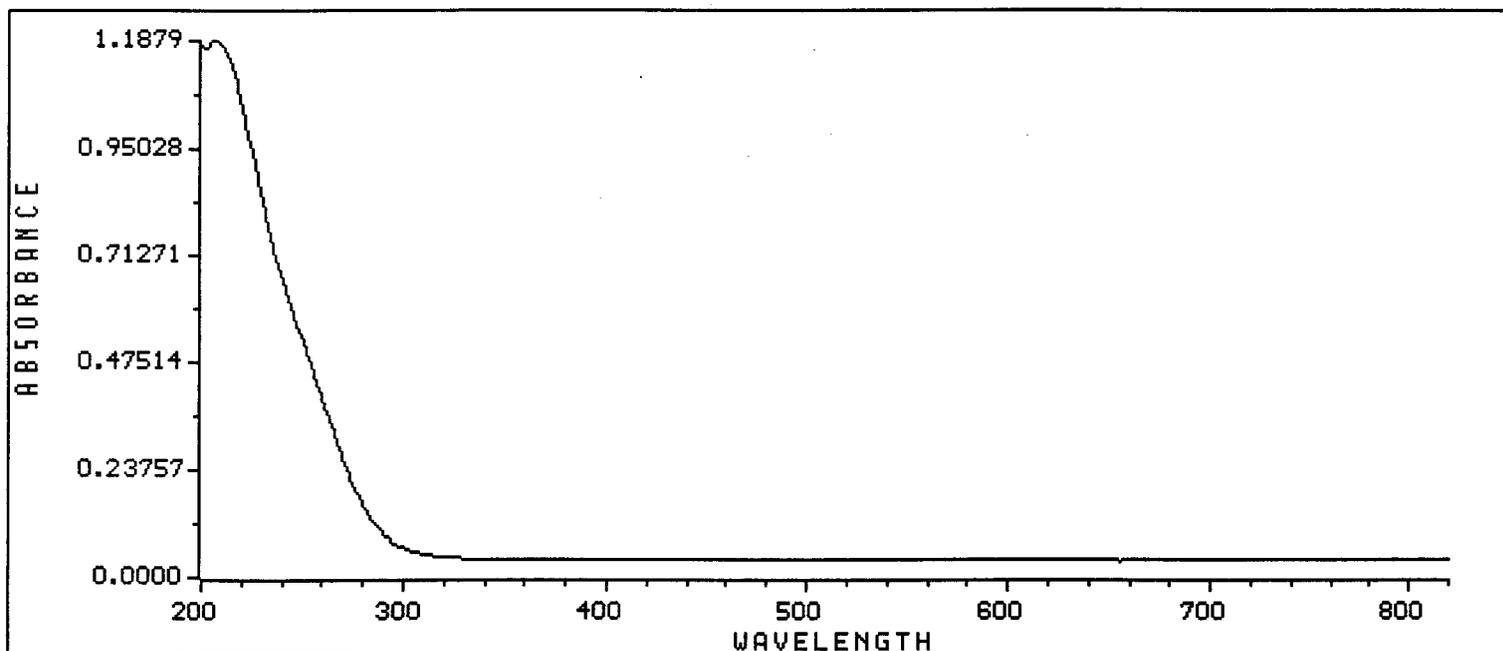
pyrex

Date   : 11-18-2002
Time   : 14:49:01
Operator : none

Sample Name : PtTFPP
Solvent Name : MeCl
Concentration :   1.0000
Units   :

Function   : Absorbance
Wavelength Range : 200 to 820 nanometers
Integration Time : 1 seconds
Std Deviation   : OFF
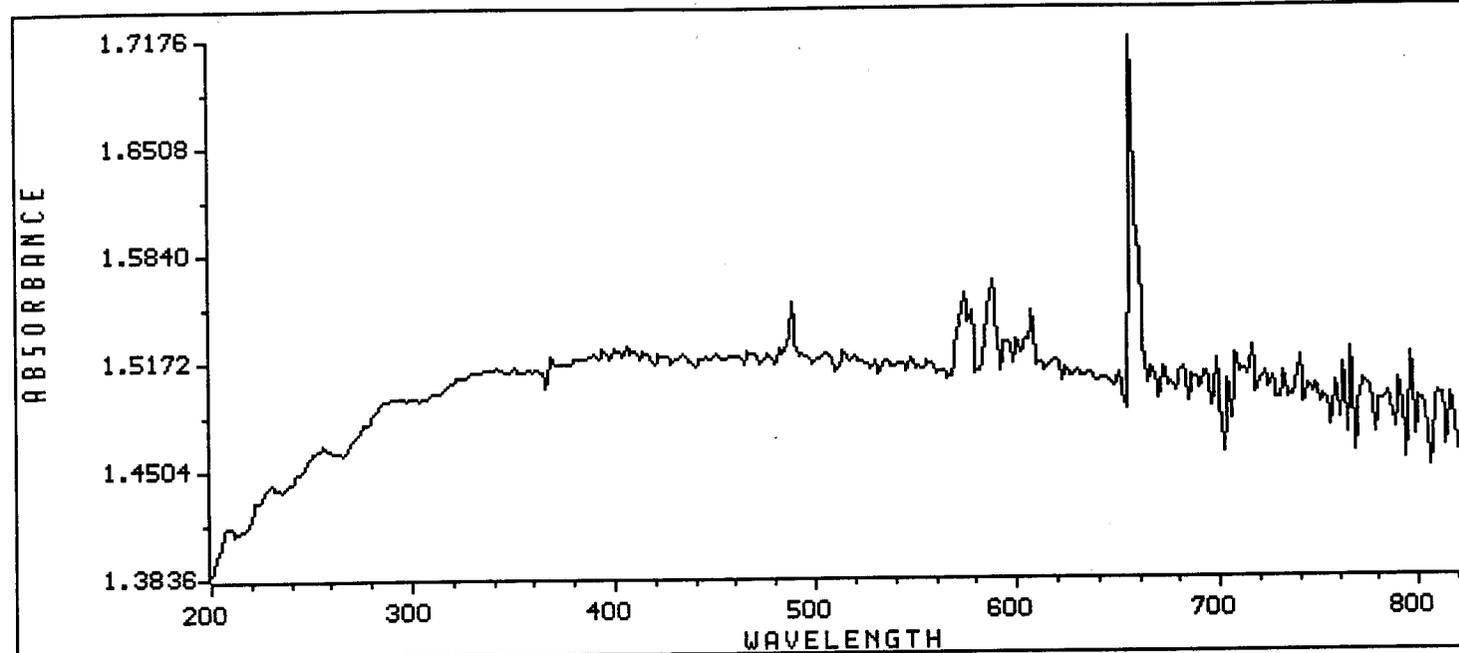
Sapphire

Date   : 11-18-2002
Time   : 14:40:31
Operator : none

Sample Name : PtTFPP
Solvent Name : MeCl
Concentration : 1.0000
Units   :

Function   : Absorbance
Wavelength Range : 200 to 820 nanometer
Integration Time : 1 seconds
Std Deviation   : OFF

Si
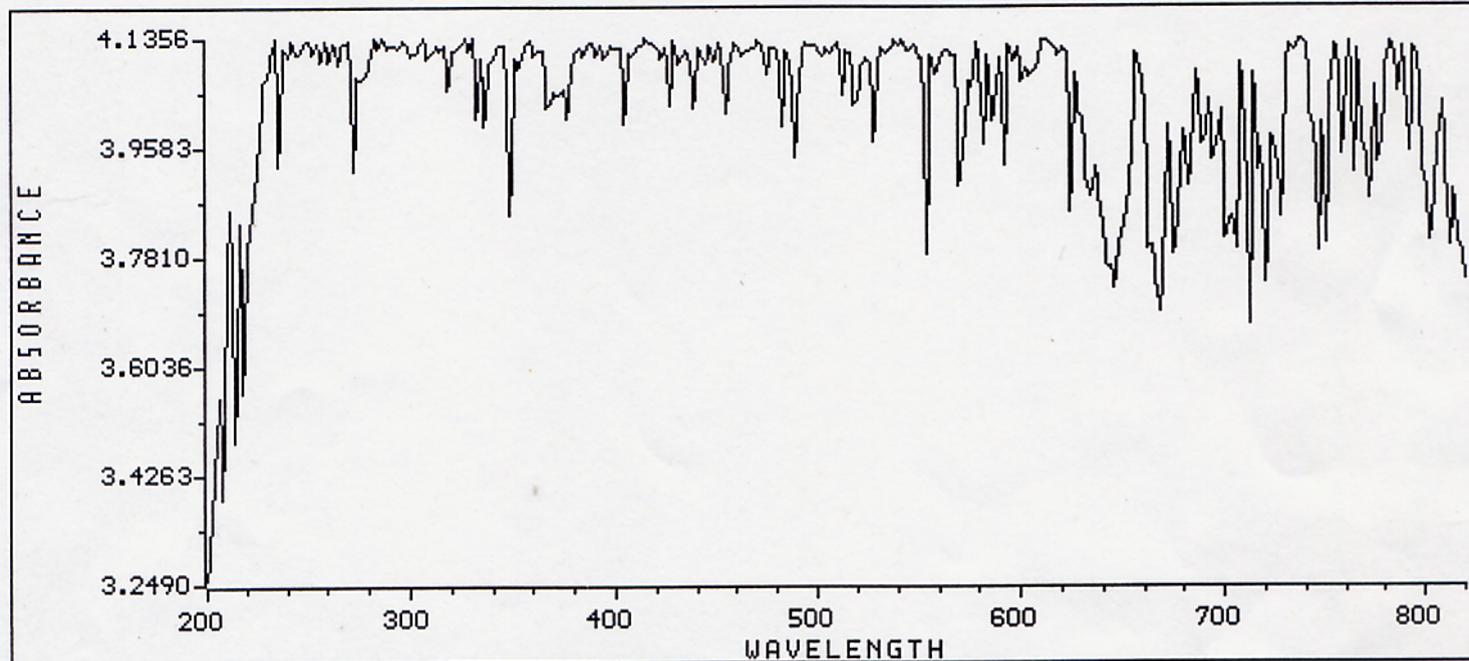
Sample Name : PtTFPP
Solvent Name : MeCl
Concentration :   1.0000
Units   :

Function   : Absorbance
Wavelength Range : 200 to 820 nanometers
Integration Time : 1 seconds
Std Deviation   : OFF
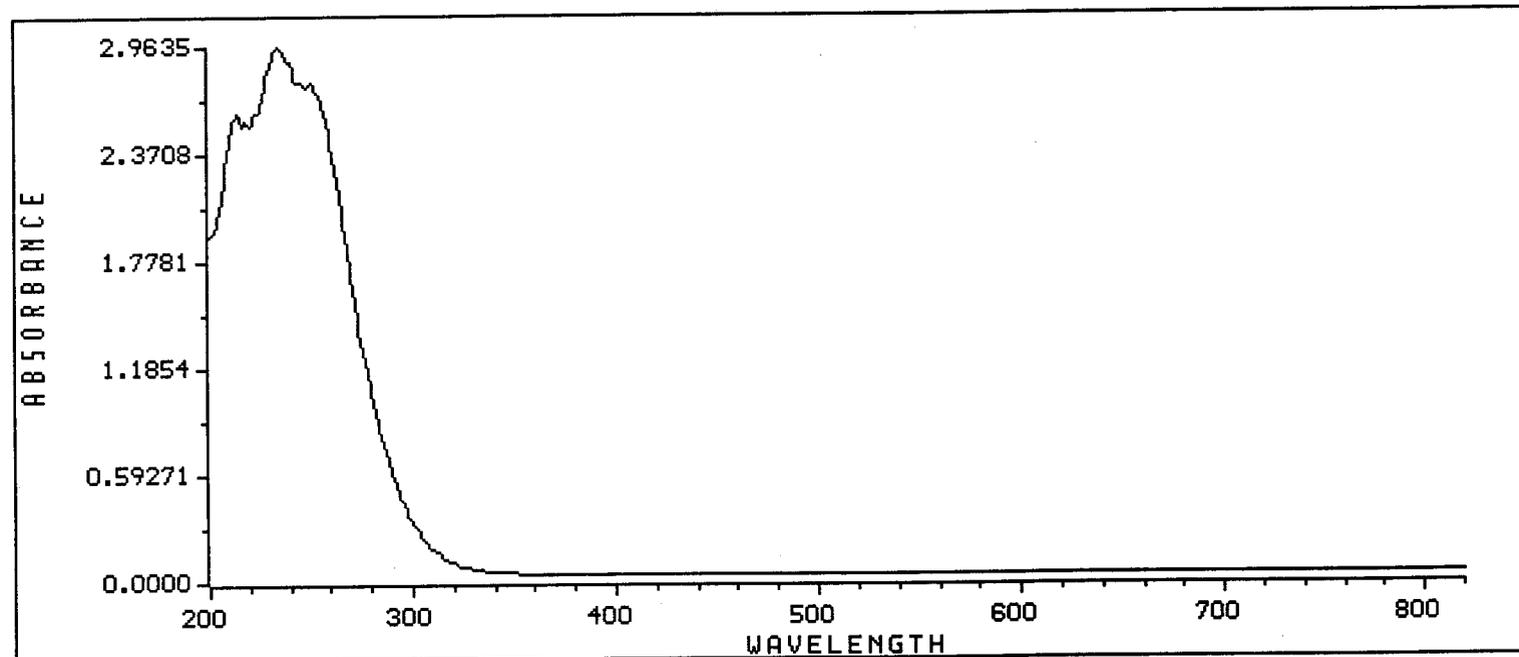
Soda lime

APPENDIX B: ESI 4440 w/ LWE 210 laser details

LWE 210

355 nm   No BXP

$2w_o \approx 0.22\,mm$ $z_{2w_0} \approx -320\,mm$
w.r.t front bezel

$\Phi_{in} \approx 2.7\,mm$

$\phi \equiv$ diameter

$\Phi_{SS}^{f=50mm} = 8.5\,mm$

$\Phi_{SS}^{f=25mm} = 4.2\,mm$

Calculated @ Obj Lens @ 1m
w.r.t from laser front bezel

355 nm   w/ 3.7x BXP

$\Phi_{in} \approx 3.2\,mm$

$\Phi_{SS}^{f=50mm} \approx 7.1\,mm$

$\Phi_{SS}^{f=25mm} \approx 3.6\,mm$

| 2x |
| $\sim 1.8\,mm$ |
| $\sim 5x$ |
| $\sim 45\,mm$ |

Calculated @
Obj lens @ 1m
w.r.t laser front bezel

Photonics DS10-266

266nm   No BXP

$2w_0 = 0.500\,mm$ $z_{2w_0} \sim -200\,mm$
w.r.t front bezel

Test Data
$z = 0.9m \Rightarrow$
w.t. laser
front bezel

x	y
1.25 mm	1.43 mm

266nm w/ 4x BXP

$\Phi_{in} \approx 2.0\,mm$

$\Phi_{SS}^{f=50mm} = 8.4\,mm$

$\Phi_{SS}^{f=25mm} = 4.2\,mm$

Calculated @ obj lens
@ 1m w.r.t. laser front bezel.

$$\Phi_{SS} \gtrsim \frac{4}{\pi} \frac{\lambda f}{\Phi_{in}}$$

Perfect TEM$_{00}$ case!.

Lightwave 355 nm

210 - V06   5.0w (500 ns))   30A

P(ω)

~3.5

x Typical perf
• spec

~1.5

10
R
    20   30

PRF=(kHz)

~20 ns

5w / 4.25 π mm² = w / cm²

A_s PRF ↑, peak power ↓, P(ω) ↓
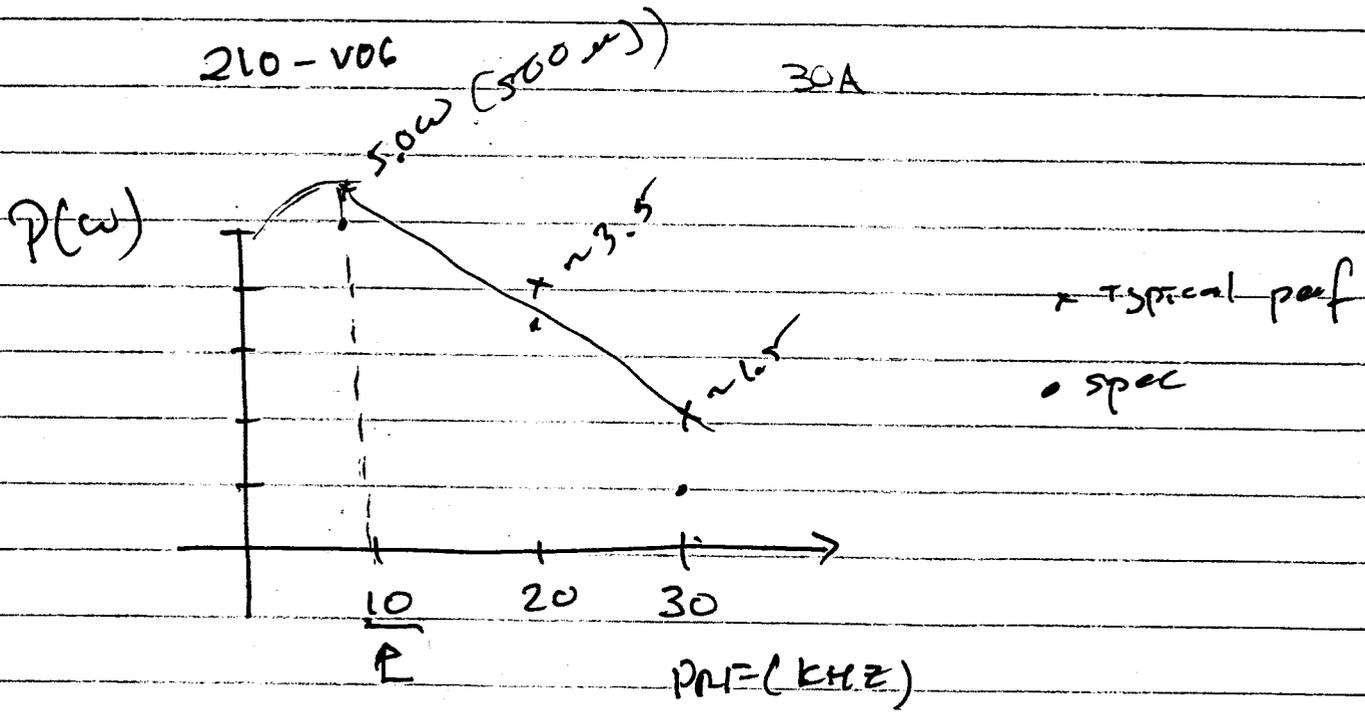
APPENDIX C: Profilometer Data & Plots

Data available upon request.